CYCLIC DEFORMATION AND FATIGUE ENDURANCE OF EN 15R STEEL UNDER MULTIAXIAL OUT-OF-PHASE LOADING

U.S. Fernando, M.W. Brown and K.J. Miller
Department of Mechanical and Process Engineering
University of Sheffield, UK

Third International Conference on Biaxial/Multiaxial Fatigue
April 3-6, 1989, Stuttgart, FRG

ABSTRACT

Multiaxial tension-torsion low cycle fatigue tests have been conducted on En15R quenched and tempered steel for both in-phase and out-of-phase loading. Two different tubular specimen geometries have been employed, and both deformation behaviour and endurance have been monitored under strain control for isotropic and anisotropic materials.

Cyclic deformation under non-proportional loading shows considerably more strain hardening than the corresponding in-phase behaviour. The stable cyclic stress-strain curve reflects the strain path adopted in a multiaxial fatigue cycle. The observed stress response is compared to out-of-phase studies on other materials, and subsequently used to assess the endurance with an equivalent strain range.

In design, correlation of multiaxial fatigue to uniaxial behaviour is usually achieved through an equivalent strain range. Different criteria are compared for both in-phase and out-of-phase loading, and related to crack propagation models through equivalent strain formulae.

INTRODUCTION

Engineering components are often subjected to cycles of severe loading and/or cyclic variations of temperature that produce inelastic deformation in critical sections. Design of such components is essentially based on knowledge of high strain fatigue and therefore also involves analysis of elastic-plastic response. The reliability of the design depends largely on the accuracy of the constitutive models and hardening laws used in the deformation analysis, as well as the validity of the fatigue failure criterion used.

In general, fatigue design data are generated from simple uniaxial tests. Many experimental investigations have examined high strain fatigue and cyclic stress-strain behaviour under combined axial-torsional loading, providing deformation and fracture criteria for correlation of multiaxial fatigue effects to uniaxial behaviour. Actual components in engineering practice however are often subjected to complex multiaxial loading, i.e. the individual principal components of the stress/strain state vary non-proportionally and the principal directions change continuously during a cycle of loading. The adequacy of such criteria has not been verified for wide ranges of non-proportional loading conditions.

In this investigation, various cyclic deformation models and fatigue criteria are assessed for in-phase and out-of-phase high strain fatigue tests conducted on En15R steel. Two batches, one isotropic and one anisotropic, are used to investigate specific effects of material anisotropy. Tests also have been conducted using two different specimens to elucidate specimen geometry influences.

CYCLIC DEFORMATION BEHAVIOUR

A stress-strain curve may be defined by the amplitudes of stress and strain measured from stabilised hysteresis loops. This is usually used to characterise the cyclic deformation behaviour of materials. It has increasingly been accepted by engineering designers as the appropriate strain hardening law for high strain fatigue analysis. Furthermore in multiaxial fatigue, deformation models are defined with an appropriate yield criterion so that a single cyclic stress-strain curve can be used, which will correlate test data obtained for all multiaxial strain states.

Usually the cyclic stress-strain curve is expressed as a power law hardening equation:

$$\tau^* = K\left(\frac{\gamma^*}{2}\right)^n \qquad [1]$$

where K and n are the cyclic strength coefficient and cyclic strain hardening exponent respectively, and τ^* and γ^* are shear stress and shear strain measures, defined by the governing yield criterion. For pure power law hardening γ^* represents a total strain, but for a Ramberg-Osgood form γ^* represents the plastic component of strain. The most widely used deformation models are based on either maximum shear (Tresca) or octahedral shear (Mises) yield criteria.

For in-phase loading, Havard & Topper (1) employed a cyclic stress-strain curve in terms of octahedral shear stress and octahedral plastic shear strain to correlate results for mild steel over a wide range of stress biaxilities which were obtained from combined axial and pressure loading of thin tubes. The same method was used by Mackenzie et al (2) for En 25 and En 32B low alloy steels.

Brown & Miller (3) suggested that because of the formation of persistent slip bands and dislocation cell structures oriented on the maximum shear plane, a cyclic stress-strain curve in terms of maximum shear stress and maximum shear strain is more appropriate to correlate multiaxial data. This observation was verified by Kanazawa et al (4), Kandil (5) and Andrews (6) for different materials at various temperatures and strain rates.

Under non-proportional straining however, the rotation of maximum shear plane activates additional slip systems in the material by changing the preferential slip plane from one crystallogrphic slip system to another. The interaction of active slip systems on different planes (and resulting dislocation jogs) causes additional strain hardening of the material. This is commonly noticed in non-proportional tests as stabilised stresses are greater than those of corresponding in-phase tests for same strain amplitudes. For sinusoidal tension-torsion loading, the amount of additional hardening increases with the phase 1 ag, ϕ, between the axial and torsional strains, and for $\phi = 90°$ the greatest hardening is observed.

Kanazawa et al (4) proposed a modification to the strength coefficient, K in equation [1] to account for this non-proportional hardening.

$$K = K_{prop} / (1 + gF) \qquad [2]$$

where K_{prop} is the cyclic strength coefficient for proportional loading and g is an empirical material constant. The rotation factor F is defined by:

$$F = \frac{\text{shear strain range on plane at 45° to the maximum shear strain range}}{\text{maximum shear strain range}}$$

Clearly F is zero for proportional loading, but it reaches a maximum value of unity for sinusoidal straining with strain biaxility factor $\lambda = 1+\nu$ and $\phi = 90°$ where λ is the ratio of torsional to axial strain ranges. In this case all crystallographic slip planes of the material are subjected to the same range of maximum shear strain.

Kanazawa's model does not accurately represent the elastic part of the stress-strain curve since no additional hardening is observed under out-of-phase elastic loading. This, together with the observed fact that the amount of non-proportional hardening increases with strain range (4) tends to indicate that the factor g in equation [2] is not constant, but increases with strain range. Yuan and Brown (7) recently suggested that the variation of g for different materials can be attributed to the involvement of different dislocation structures in addition to the amount of plastic strain. They proposed a cyclic strain hardening rule based on maximum shear criteria to account for the non-proportional strain path effect:

$$\tau_{max} = K_s\left[\frac{\gamma_{max}}{2}\left\{1 + D\left|\frac{\gamma_{max}}{\gamma_y} - 1\right| F\right\}\right]^n \qquad [3]$$

where γ_y is the cyclic yield strain of the material and D is an empirically obtained dislocation hardening coefficient. The value of D is a measure of additional hardening caused by the underlying dislocation mechanism for the material. However, for metals that favour a Mises yield criterion under in-phase loading, Yuan's deformation model can be expressed as:

$$\tau_{oct} = K_o\left[\frac{\gamma_{oct}}{2}\left\{1 + D\left|\frac{\gamma_{oct}}{\gamma_y} - 1\right| F\right\}\right]^n \qquad [4]$$

An important feature of Yuan's model is that the non-proportional correction is applied to the strain term, compared to Kanazawa's approach where the correction is applied to the stress term. Since higher values of F represent greater accumulated strain in a cycle due to a complex straining path, the correction of the strain term may be considered as more appropriate.

EQUIVALENT STRAIN FATIGUE CRITERIA

It is generally assumed that by incorporating the governing parameters for fatigue fracture in an appropriate formula, a single endurance curve may be derived to represent all multiaxial fatigue endurance data. This concept is the basis of equivalent strain criteria. Equivalent strain relates components of a multiaxial state of strain to a corresponding primary state that gives the same fatigue endurance. Thus with knowledge of the fatigue endurance curve under uniaxial loading, the life of a component under multiaxial loading can be estimated.

A widely used example given in ASME Boiler and Pressure vessel code case N47 (8) is based on the Mises or octahedral strain, which corresponds to the

effective strain used in plasticity theory. In terms of principal strains, ε_1, ε_2 and ε_3, the Mises criterion may be written as:

$$\varepsilon_{EQ}\ \text{MISES} = \frac{1}{\sqrt{2}(1+\nu)} \left\{ (\varepsilon_1 - \varepsilon_2)^2 + (\varepsilon_2 - \varepsilon_3)^2 + (\varepsilon_3 - \varepsilon_1)^2 \right\}^{1/2} \quad [5]$$

where ν is the elasto-plastic value of Poisson's ratio. For proportional loading cases, the principal values may be represented by strain amplitudes. A more complex method is defined for non-proportional straining (8).

The Tresca or maximum shear strain criterion has been extensively used (9), which is also related to plastic deformation theory as an effective strain [3]. In terms of principal strains, this criterion can be written as:

$$\varepsilon_{EQ}\ \text{TRESCA} = \frac{1}{(1+\nu)} \left\{ \varepsilon_1 - \varepsilon_3 \right\} \quad [6]$$

where $\varepsilon_1 \geq \varepsilon_2 \geq \varepsilon_3$.

A third criterion is the Rankine equivalent strain based on maximum principal stress. It may be derived from fracture mechanics considerations of mode I cracking (10). For proportional straining, this criterion may be expressed in terms of principal strains as:

$$\varepsilon_{EQ}\ \text{RANKINE} = \sigma_1\ \gamma^* / (2\ (1+\nu)\ \tau^*)$$

$$= \frac{1}{(1+\nu)} \left\{ \varepsilon_1 + \nu(\varepsilon_1 + \varepsilon_2 + \varepsilon_3) / (1 - 2\nu) \right\} \quad [7]$$

where σ_1 is maximum principal stress.

All the above formulae, apart from their apparent simplicity, do not involve any empirical constants. Therefore these criteria can be used with reference to endurance data from a single primary loading.

Brown & Buckthorpe (10) proposed an equivalent strain criterion for triaxial loading, based on crack propagation mechanisms,

$$\varepsilon_{EQ}\ \text{TRIAX} = \varepsilon_{EQ}\ \text{RANKINE} + \sqrt{\varepsilon_o \cdot \varepsilon_{EQ}\ \text{TRESCA}}\ \left(1 - \frac{\varepsilon_{EQ}\ \text{RANKINE}}{\varepsilon_{EQ}\ \text{TRESCA}}\right) \quad [8]$$

with the constant $\varepsilon_o = 2\varepsilon_{f1}Q\left(\frac{1}{Q} - 1\right)^2$, where Q is the ratio of the torsional and uniaxial fatigue strengths at the fatigue limit and ε_{f1} is the uniaxial

strain amplitude at the fatigue limit. The important feature of this criterion is that it takes account of the two crack growth phases, stage I and stage II, which comprise fatigue life. Near the fatigue limit, stage I crack growth is predominant and thus fatigue life is related to maximum shear strain, but at high strain levels the stage II growth phase is dominant and endurance is related to maximum principal stress. Equation [8] is weighted to reflect these mechanisms, but it requires the value of Q as well as endurance data for a single primary loading mode.

For tension-torsion non-proportional straining, Andrews (6) proposed an empirical equivalent strain criterion

$$\gamma_{EQ}\ \text{ANDREWS} = \gamma_{max} + \frac{2\ S\ \varepsilon_n}{(1 + BF)} \qquad [9]$$

where ε_n is the normal strain amplitude on the plane of highest maximum shear range, and B and S are empirical constants. The rotation factor F is defined above. The value of S is estimated by comparing in-phase endurance data for two distinct primary loadings. The value of B can be found by fitting at least one non-proportional data point, preferably the one with greatest hardening. Andrews criterion is based on the two parameter approach originally proposed by Brown & Miller (1) which identified the strain parameters that control fatigue fracture.

Recently, Yuan and Brown (12) proposed an equivalent strain criterion based on Tomkins mode I crack growth theory, i.e. crack growth rate is proportional to $\sigma_1^2\ \gamma_{max}$. For tension-torsion loading, using the cyclic stress-strain relation given in Equation [3], they derived the equivalent strain,

$$\gamma_{EQ}\ \text{YUAN} = \gamma_{max}\left[\left\{(1 + \nu)\ \frac{\varepsilon}{\gamma_{max}} + 1\right\}\left\{1 + D\ \left|\ \frac{\gamma_{max}}{\gamma_y} - 1\ \right|\ F\right\}^n\right]^{\frac{2}{1 + 2n}} \qquad [10]$$

where ε is axial strain. The important feature of this criterion is that it requires only the full cyclic stress-strain curve and an endurance curve for a single primary loading mode.

MATERIAL AND TEST PROGRAMME

To evaluate the effectiveness of different deformation models and equivalent strain criteria, high strain fatigue experimental data obtained on En15R quenched and tempered steel for wide range of complex multiaxial loading waveforms are assessed using these theories.

Two batches of material were supplied in the form of extruded cylindrical bars. The first batch had a high sulphur content of 0.047%, which formed MnS inclusions in a rod-like shape (about 500μm in length and 5μm in diameter) aligned with the bar axis. The second batch had a low sulphur content of 0.004%, rendering a microstructure free of long MnS inclusions. Due to the above microstructural feature, the first batch of the material was found to be anisotropic in fatigue behaviour.

The specimen was of tubular geometry with 30mm guage length, 22mm nominal outside diameter and 16mm nominal bore. The bore was finished by honing and the outside surface polished to a consistent finish. Tests were also conducted on the anisotropic batch using a different fatigue machine and a tubular geometry of 20mm parallel length, 20mm outside diameter and 16mm bore.

Both specimens were subjected to combined axial and torsional strain controlled loading. The test machines employed are described by Brown and Miller (13) and Fernando (14). Axial and torsional strains were directly controlled from an extensometer attached across the gauge length. Command signals for each servo system were generated using a twin-channel waveform generator, with an adjustable phase shift.

The amplitudes of loading in fully reversed biaxial tests were selected in the low-cycle fatigue regime. Sinusoidal waveforms were used with a frequency selected to achieve a maximum shear strain rate of approximately 0.1% per sec. The load and strain histories were recorded on a multi-pen chart recorder and load-strain hysteresis loops were periodically recorded using X-Y plotters. Specimen failure was identified from either an axial load range or a torque range drop of 2% from their respective stabilised values.

RESULTS

The deformation and endurance results of all in-phase and out-of-phase tension-torsion tests are presented in Figs. 1 to 5. The strains are given in terms of amplitudes and the stresses were derived from the loads measured at instants when the maximum shear strain was highest in a loading cycle.

The outer surface axial and torsional stresses were obtained from the respective loads by a procedure based on the Prandtl-Reuss equations for incremental plasticity, applicable to both in-phase and out-of-phase loading (6, 7). During analysis the elasto-plastic Poisson's ratio was calculated from the method suggested in Ref. 8.

The cyclic stress-strain curve and the endurance curve derived from uniaxial data alone are expressed as

$$\varepsilon = \frac{\sigma}{E} + \left(\frac{\sigma}{K_u}\right)^{1/n} \quad [11]$$

$$\varepsilon = \frac{\sigma_f'}{E}(2N_f)^b + \varepsilon_f'(2N_f)^c \quad [12]$$

The values of the constants for the isotropic and anisotropic batches of the material are given in Tables I and II. For both materials Young's Modulus, the elastic Poisson's ratio and yield strain in shear were taken as 205 GPa, 0.28 and 0.268% respectively, and the uniaxial fatigue limit was taken as $\pm$ 373 MPa. The fatigue limit ratio Q was assumed to be 0.6 (10).

DISCUSSION

The correlation of deformation data for isotropic and anisotropic batches of material on the basis of maximum shear, octahedral shear and Yuan's modified maximum and octahedral shear models, are shown in Figs. 1 and 2 respectively. As clearly seen, for both batches the Mises or octahedral shear criterion is superior in correlating in-phase data. This was also observed by Yang (15). The line in each figure represents the uniaxial curve given by Equation [11]. The isotropic material shows slightly higher strength compared to the anisotropic material.

For both batches of material, out-of-phase data show considerably more strain hardening than in-phase data. This is more apparent when the data are compared on the basis of maximum shear. Due to the additional hardening, out-of-phase results cannot correlate well on the basis of maximum shear or octahedral shear criteria. However, Yuan's modification of the octahedral shear criterion given in Equation [4] is successful in correlating additional hardening effects caused by non-proportional straining paths. Approximately the same dislocation hardening coefficient 0.278 for the isotropic material and 0.305 for the anisotropic material indicates that dislocation structure of the material is not significantly affected by the presence of MnS inclusions.

Figure 3 compares the cyclic deformation data obtained from two specimen geometries, on the basis of equation [4]. Results from both specimens correlate well, as plastic deformation is caused by slip in individual grains and is not influenced by wall thickness. The lower stress associated with the uniaxial specimen (S2) at 0.7% strain may be due to incipient buckling of this thin wall specimen.

The fatigue endurance data of isotropic and anisotropic materials are presented in Figs. 4 and 5 respectively, on the basis of the different equivalent strain criteria given in equations [5] to [10]. Distinct fatigue endurance behaviour is observed for two batches of the material. For the triaxial equivalent strain, non-proportional loading cases are treated as if the axial and torsional applied strains were in-phase to give an artificially high strain amplitude to allow for the observed life reduction (10). The same procedure has been used for the Tresca, Mises and Rankine criteria.

For isotropic material the deformation based criteria, Tresca and Mises, have the highest scatter, and the triaxial criterion has less scatter. Andrews' empirical criterion with S = 1.38 and B = 0.6, shows a good correlation. The Rankine criterion and Yuan's model correlated data well, except for torsion. On the contrary, for the anisotropic material, the Tresca and Mises criteria show lower scatter for in-phase data, and Mises criterion is slightly superior. Andrews' criterion with S = 0.4 and B = -0.4 shows good correlation for both in- and out-of-phase data. All other criteria are good except for out-of-phase loading, in-phase loading with high values of λ, and torsion.

Observation of fractured specimens by Yang (15) revealed that two distinct crack growth modes occur in this material depending on strain biaxiality ratio λ. Failure by mode I cracks was observed for loading cases closer to uniaxial and failure by mode III cracks occurred close to torsion. The transition of fracture mode from mode I to mode III was at about $\lambda = 3$ for the isotropic batch, and at about $\lambda = 1.5$ for the anisotropic batch. Failure by mode III cracking is observed for all non-proportional tests. Comparison of endurance data for both materials indicates that for mode I crack growth cases endurance is slightly affected by material anisotropy. However for mode III cracking, fatigue endurance is lowered by anisotropy. Long MnS inclusions aligned with the mode III crack orientation and severe plastic strain incompatibility at the inclusion-matrix interface, favour formation of long shallow mode III cracks. This causes a significant reduction of endurance by anisotropy for mode III cracking cases.

The endurance data highlight three important facts. Firstly, deformation based equivalent strain criteria are unsuitable for predicting fatigue endurance data. Secondly, the equivalent strain criteria developed on the basis of crack growth mechanics are more appropriate. Thirdly, in the presence of material anisotropy, enhanced crack nucleation along inclusions in torsion may

lead to the wrong conclusion that deformation based equivalent strain expressions are superior for correlation of endurance data. Most, if not all, biaxial fatigue investigations conducted in the past have employed specimens machined from extruded bars, and the inevitable presence of anisotropy in such material may be a significant factor in the prevalent view favouring deformation based criteria.

The crack growth based equivalent strain criteria, namely the Rankine expression and Yuan's model, correlate fatigue endurance for loading cases dominated by mode I crack growth. However, these criteria break down when crack growth modes other than mode I occur.

Both the triaxial and the Andrews approaches have an ability to allow for anisotropy. If Q is determined for both materials, then the anisotropic material will have a higher value of ε_o, raising the torsion and out-of-phase data points towards the uniaxial lines. In the Andrews expression, S and B are selected to fit uniaxial, torsion and non-proportional data, and therefore this gives the best correlation for both materials.

Figure 5 also compares endurance data for anisotropic material obtained using two specimen geometries. It can be seen that the endurance is not significantly affected by specimen size.

CONCLUSIONS

1. For both batches of En15R, in-phase deformation data are correlated by the octahedral shear criterion

2. The additional strain hardening observed in out-of-phase loading is described by a strain path correction.

3. Deformation based equivalent strain criteria are unsatisfactory for correlation of fatigue endurance.

4. Equivalent strain criteria based on crack growth aspects are satisfactory only for mode I crack growth cases.

5. Two equivalent strain criteria considered are able to correlate both mode I and mode III crack growth cases by incorporating torsional fatigue strength data in fitted constants.

ACKNOWLEDGEMENTS

The authors gratefully acknowledge W. Yang and A. Navarro for use of their experimental results. Thanks are also due to Austin Rover for the material; to the EEC for sponsorship through a BRITE programme; and to SERC for financial assistance.

REFERENCES

1. Havard D.G. and Topper T.H., "A criterion for biaxial fatigue of mild steel at low endurance", Proc. 1st Int. Conf. on Structural Mechanics in Reactor Technology, Berlin 1972, Vol. 6, pp 413-432.

2. Mackenzie C.T., Burns D.J. and Benham P.P., "A comparison of uniaxial and biaxial low endurance fatigue behaviour of two steels", Proc. Instn. Mech. Engrs., 1965-66 180 (31), pp 392-402.

3. Brown M.W. and Miller K.J., "Biaxial cyclic deformation behaviour of steels", Fat. Engg. Mater. Struct. 1979, 1, pp 93-106.

4. Kanazawa K., Miller K.J. and Brown M.W., "Cyclic deformation of 1% Cr-Mo-V steel under out-of-phase loads", Fat. Engg. Mater. Struct., 1979, 2, pp 217-222.

5. Kandil F.A., "Time effects on biaxial fatigue at elevated temperatures", Ph.D. Thesis, University of Sheffield, UK, 1984.

6. Andrews R.M. "High temperature fatigue of AISI 316 stainless steel under complex biaxial loading, Ph.D. Thesis, University of Sheffield, UK, 1986.

7. Yuan L. and Brown M.W., "Out-of-phase cyclic deformation of type 316 stainless steel", to be published 1989.

8. ASME - Boiler and Pressure Vessel code case N47-22, ASME, New York, 1984.

9. BS 5500 - Specification for unfired fusion welded pressure vessels, BSI, London, 1982.

10. Brown M.W. and Buckthorpe D.E., "A crack propagation based equivalent strain", in Biaxial and Multiaxial Fatigue, EGF Publication No. 3, Mechanical Engineering Publications, 1988, pp 499-510.

11. Brown M.W. and Miller K.J. "A theory for fatigue failure under multiaxial stress-strain conditions", Proc. Instn. Mech. Engrs., 1973, 187, pp 745-755.

12. Yuan L. and Brown M.W. "Non-proportional low cycle fatigue endurance of a stainless steel", to be published 1989.

13. Brown M.W. and Miller K.J., "A biaxial fatigue machine for elevated temperature testing", J. Testing and Evaluation, 9, 1981, pp 202-208.

14. Fernando U.S., "A new multiaxial fatigue testing facility", Ph.D. Thesis, University of Sheffield UK, 1987.

15. Yang W., Brown M.W. and Miller K.J., "Effect of material anisotropy on the biaxial fatigue behaviour of En15R steel", to be published 1989.

TABLE I Material Constants for Uniaxial Behaviour

Batch	K_u (MPa)	n	σ_f' (MPa)	ε_f'	b	c
isotropic	1438	0.189	1114	0.259	-0.097	-0.515
anisotropic	1543	0.208	1407	0.487	-0.127	-0.575

TABLE II Material constants for biaxial behaviour

Batch	D for Eq. 3	D for Eq. 4	K_o (MPa)	K_s (MPa)	S	B
isotropic	0.368	0.278	853	759	1.38	0.6
anisotropic	0.472	0.305	918	819	0.4	-0.4

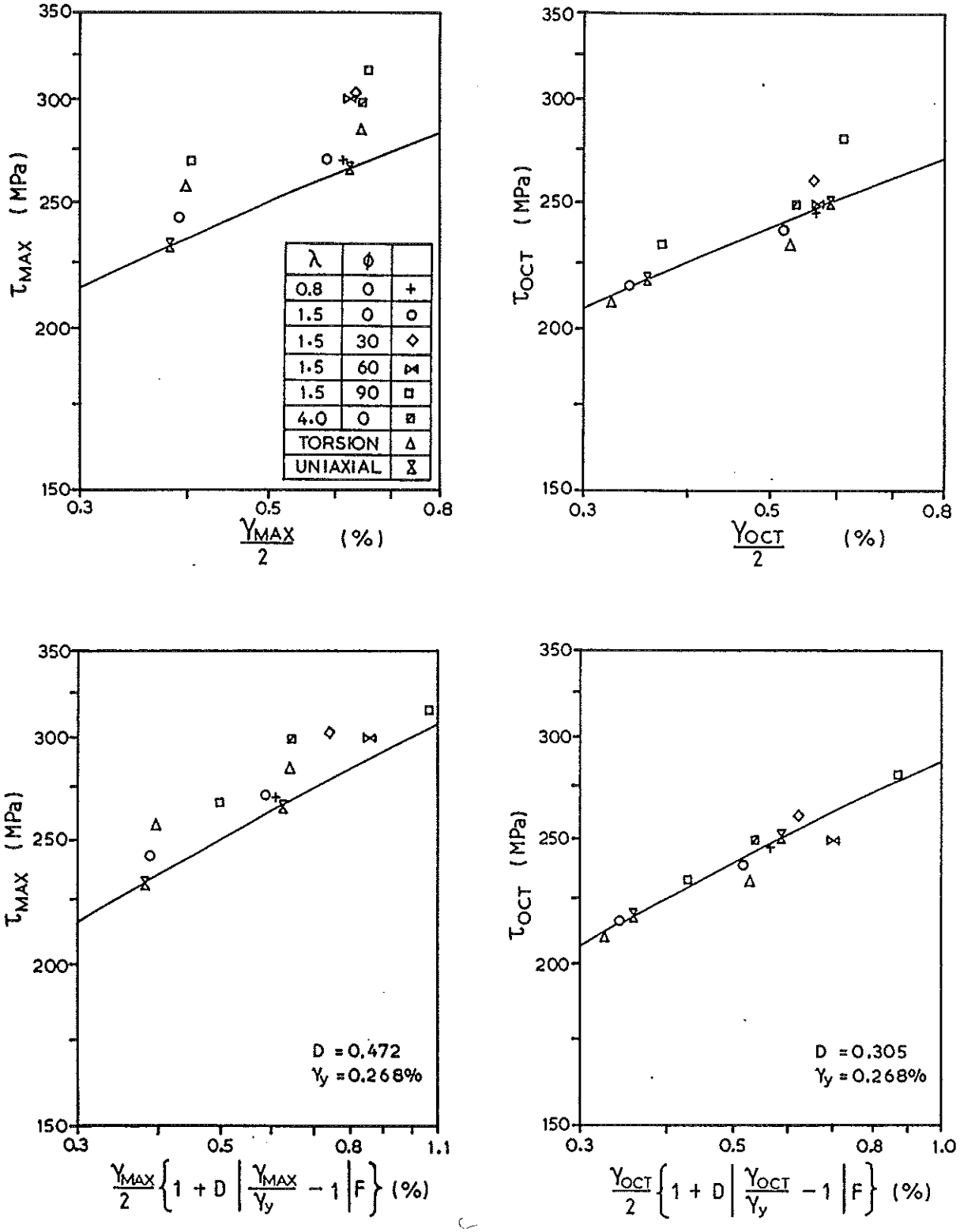

FIGURE 1. CYCLIC STRESS-STRAIN CURVE FOR THE ISOTROPIC STEEL.

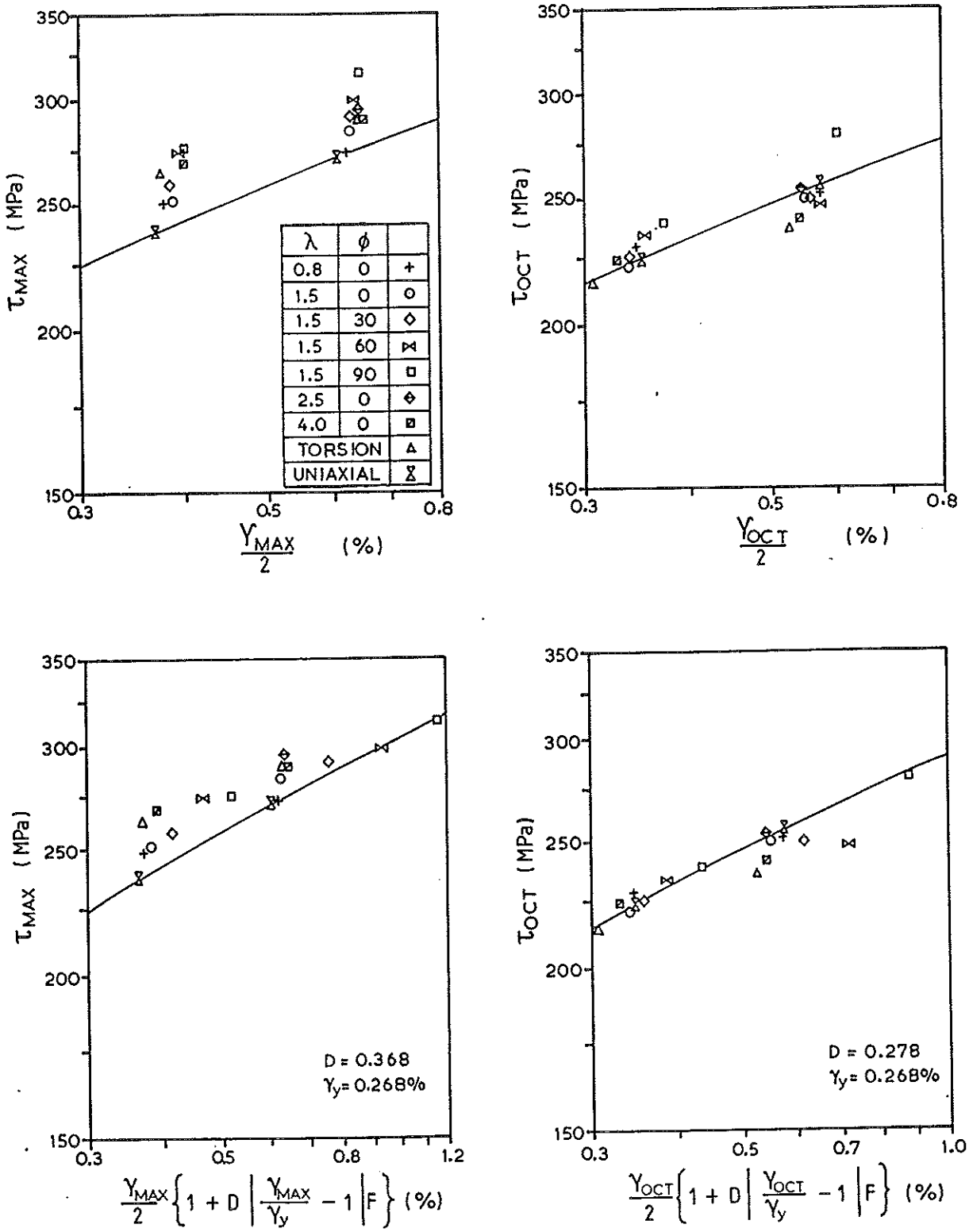

FIGURE 2. CYCLIC STRESS-STRAIN CURVE FOR THE ANISOTROPIC STEEL.

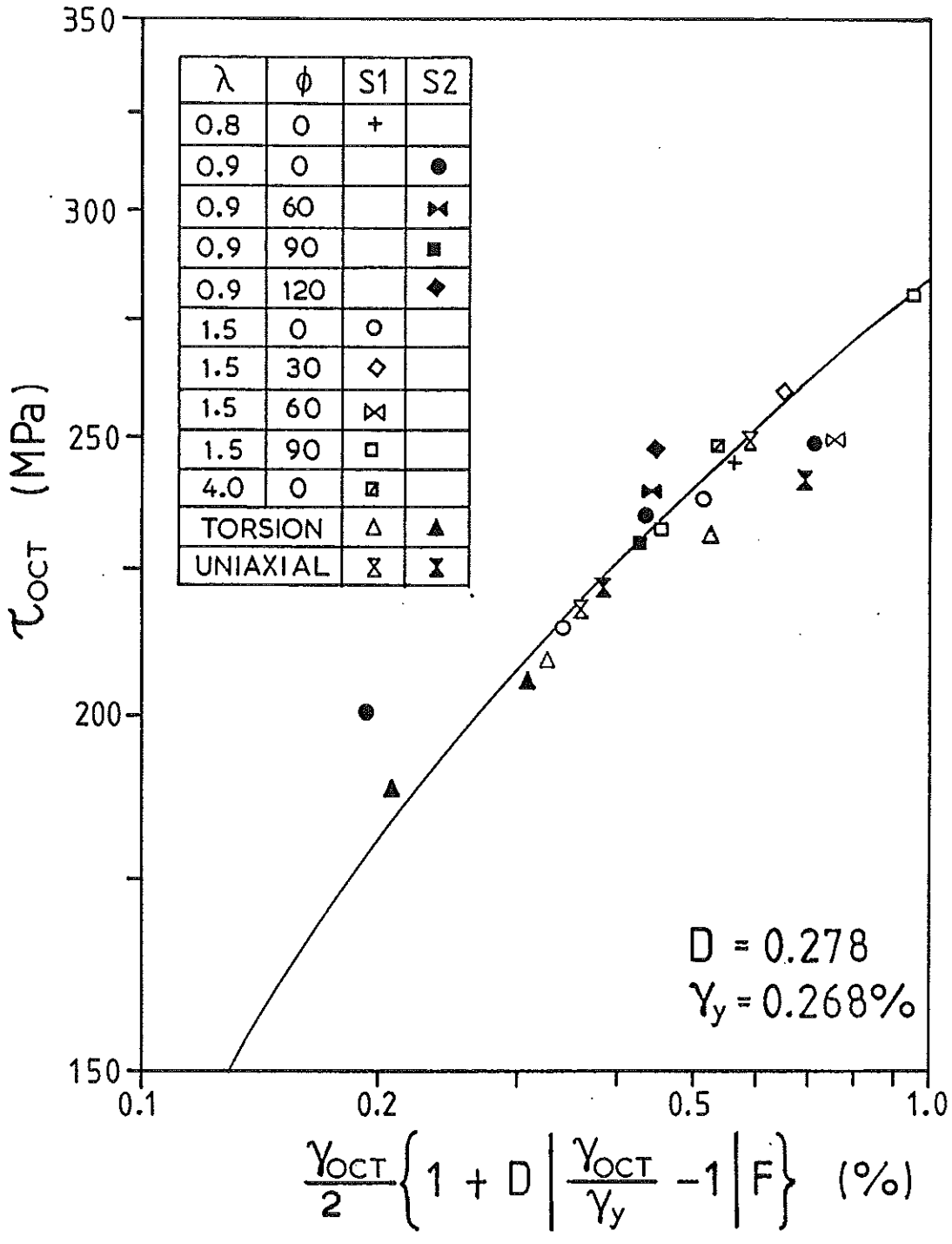

FIGURE 3. CYCLIC STRESS-STRAIN CURVE FOR THE ANISOTROPIC STEEL FOR BOTH SPECIMEN GEOMETRIES.
(S1 - SPECIMEN GEOMETRY 1; S2 - SPECIMEN GEOMETRY 2)

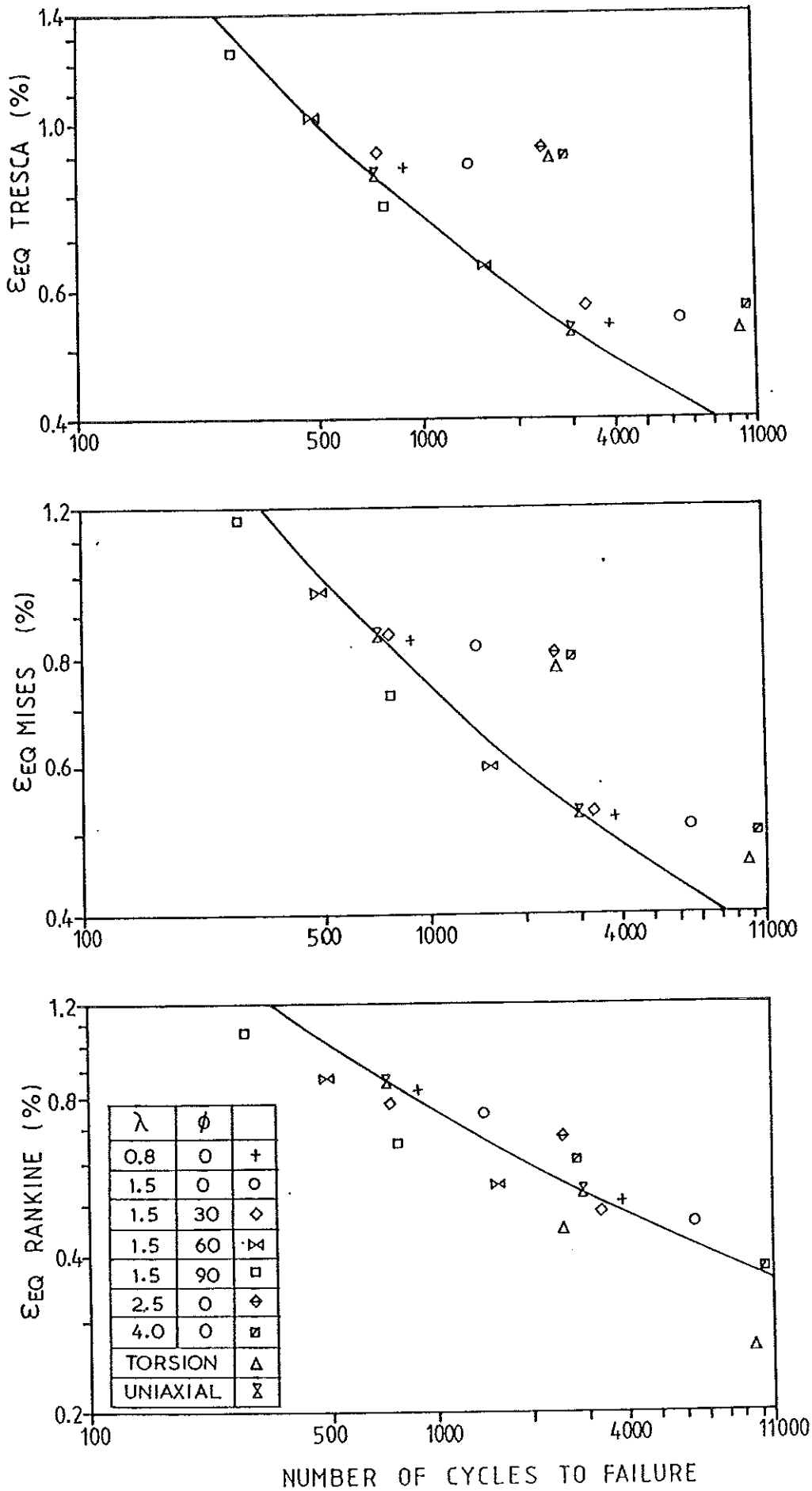

FIGURE 4. EQUIVALENT STRAIN - FATIGUE LIFE CURVES FOR THE ISOTROPIC STEEL.

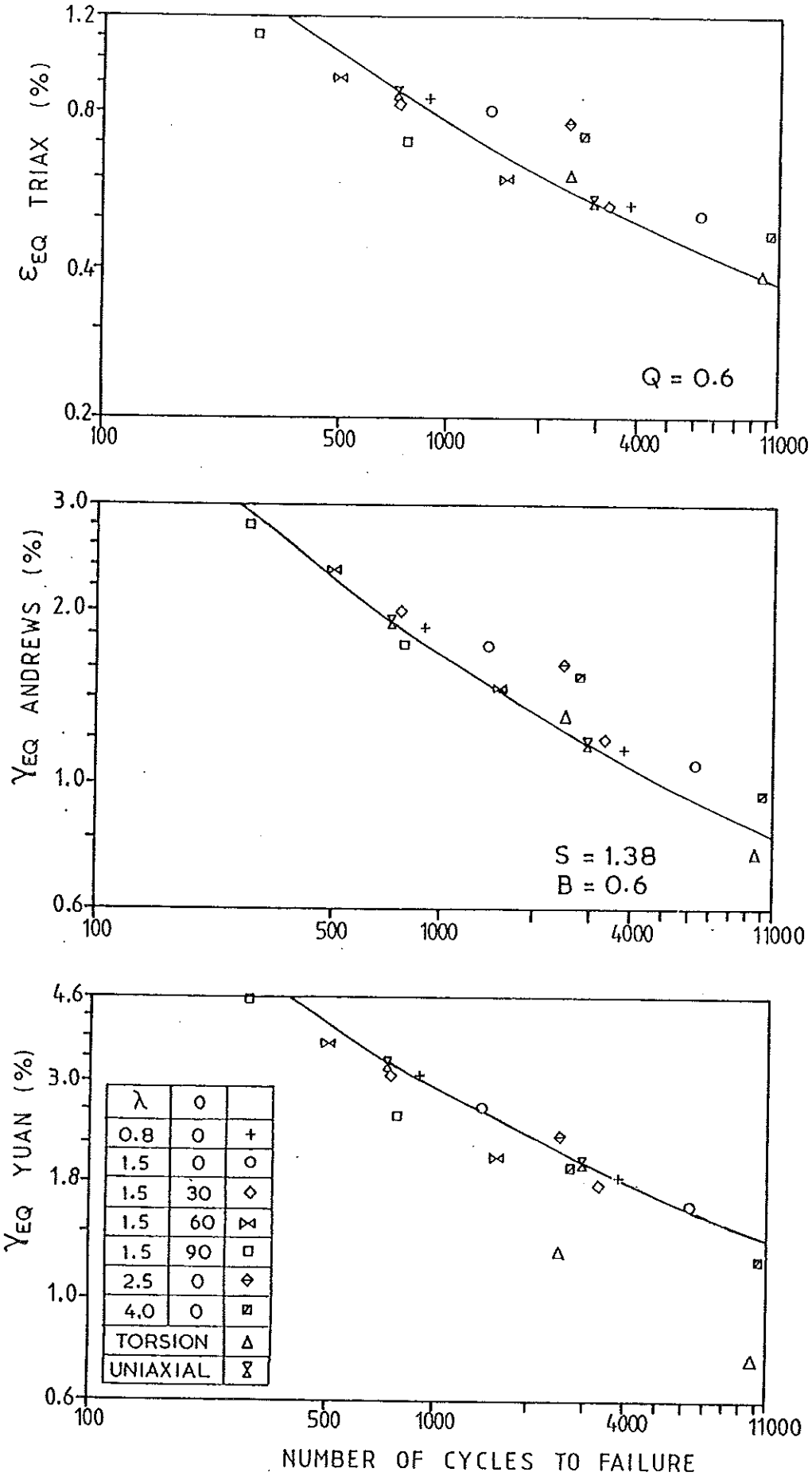

FIGURE 4. (CONTINUED).

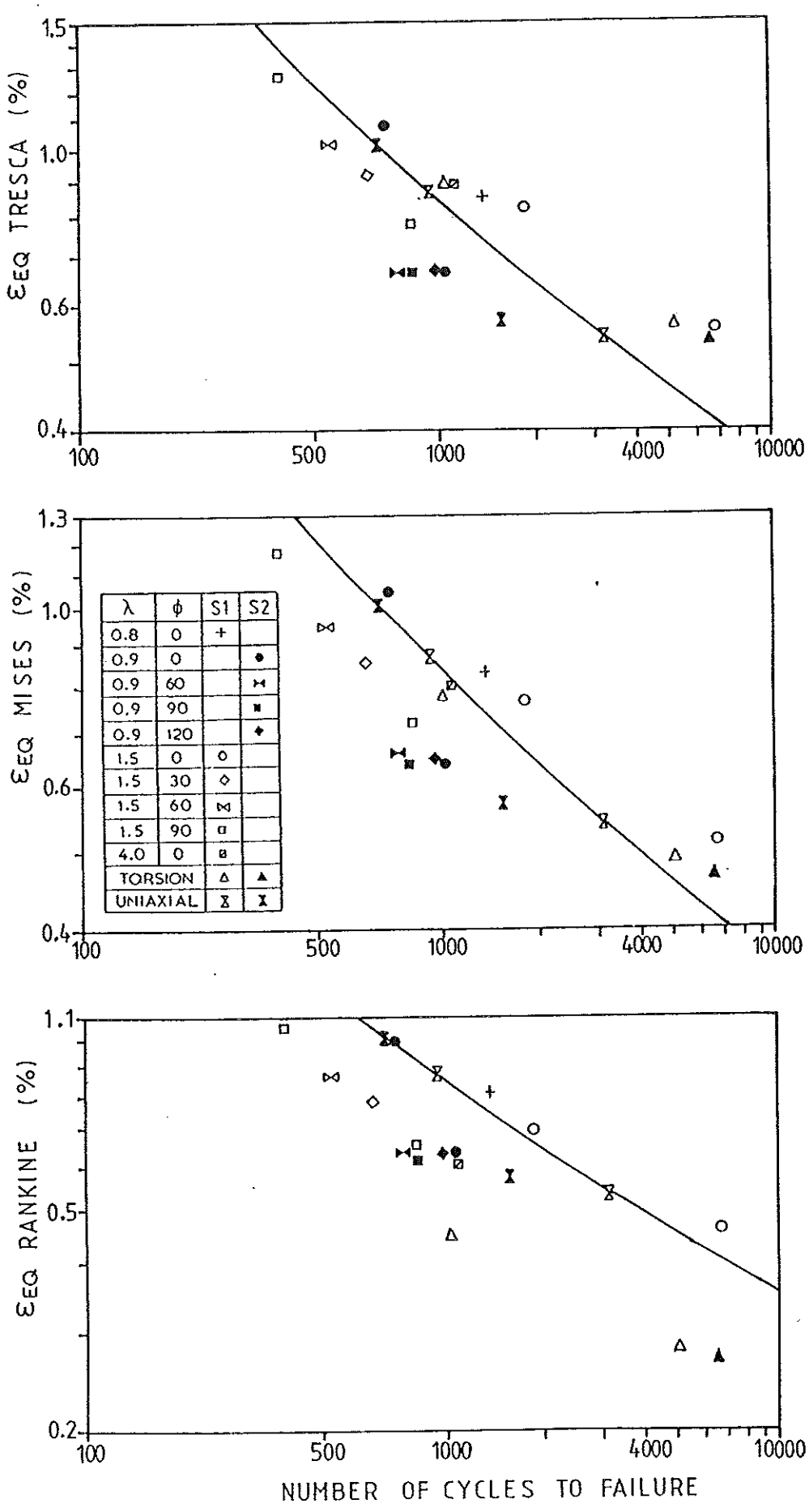

FIGURE 5. EQUIVALENT STRAIN - FATIGUE LIFE CURVES FOR THE ANISOTROPIC STEEL.

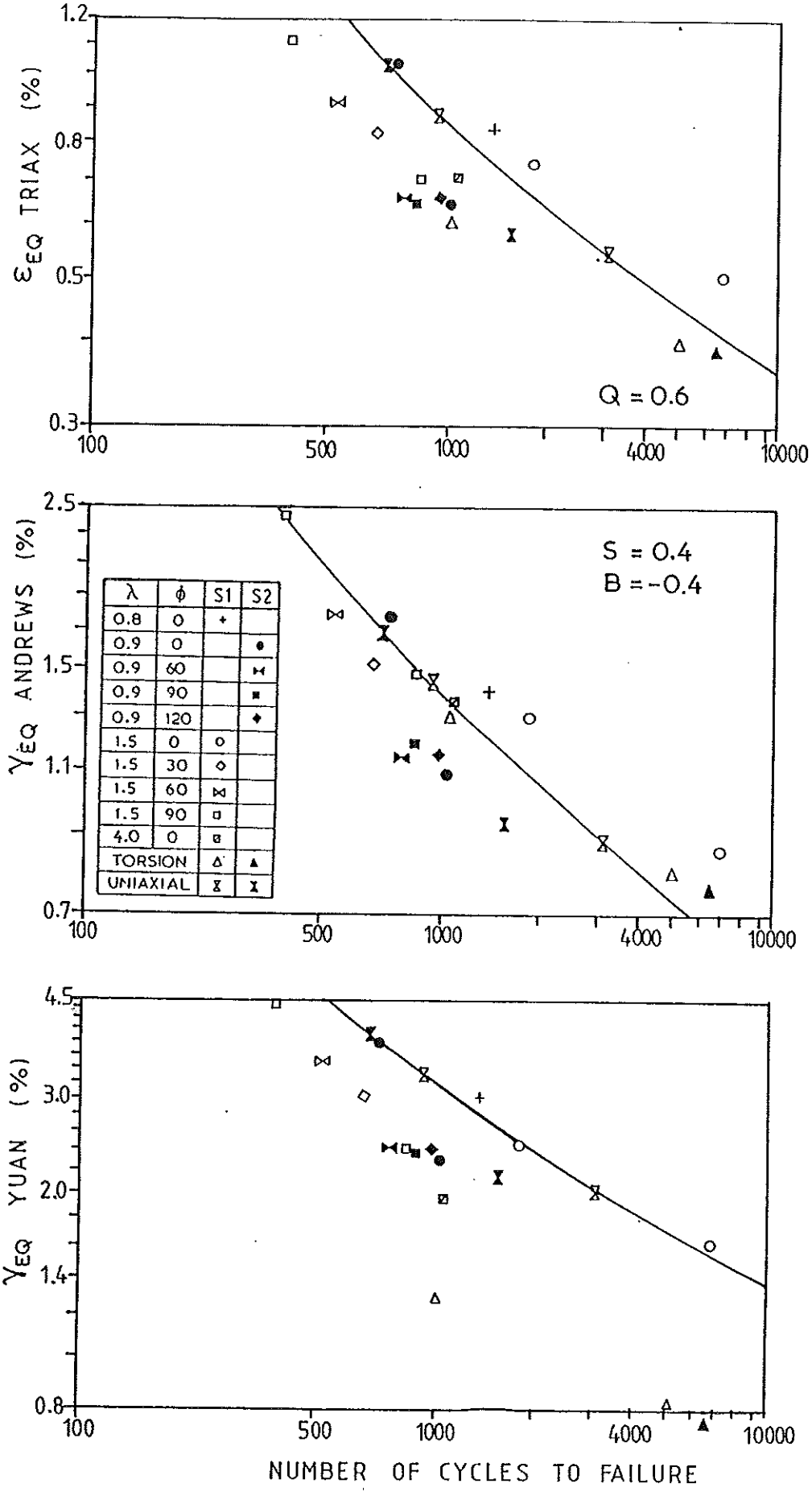

FIGURE 5. (CONTINUED).